Research Paper

PAIN®

Neuroinflammation of the spinal cord and nerve roots in chronic radicular pain patients

Daniel S. Albrecht[a,b], Shihab U. Ahmed[c], Norman W. Kettner[d], Ronald J.H. Borra[e,f], Julien Cohen-Adad[g,h], Hao Deng[i], Timothy T. Houle[i], Arissa Opalacz[c], Sarah A. Roth[c], Marcos F. Vidal Melo[i], Lucy Chen[c], Jianren Mao[c], Jacob M. Hooker[a], Marco L. Loggia[a], Yi Zhang[c,*]

Abstract

Numerous preclinical studies support the role of spinal neuroimmune activation in the pathogenesis of chronic pain, and targeting glia (eg, microglia/astrocyte)- or macrophage-mediated neuroinflammatory responses effectively prevents or reverses the establishment of persistent nocifensive behaviors in laboratory animals. However, thus far, the translation of those findings into novel treatments for clinical use has been hindered by the scarcity of data supporting the role of neuroinflammation in human pain. Here, we show that patients suffering from a common chronic pain disorder (lumbar radiculopathy), compared with healthy volunteers, exhibit elevated levels of the neuroinflammation marker 18 kDa translocator protein, in both the neuroforamina (containing dorsal root ganglion and nerve roots) and spinal cord. These elevations demonstrated a pattern of spatial specificity correlating with the patients' clinical presentation, as they were observed in the neuroforamen ipsilateral to the symptomatic leg (compared with both contralateral neuroforamen in the same patients as well as to healthy controls) and in the most caudal spinal cord segments, which are known to process sensory information from the lumbosacral nerve roots affected in these patients (compared with more superior segments). Furthermore, the neuroforaminal translocator protein signal was associated with responses to fluoroscopy-guided epidural steroid injections, supporting its role as an imaging marker of neuroinflammation, and highlighting the clinical significance of these observations. These results implicate immunoactivation at multiple levels of the nervous system as a potentially important and clinically relevant mechanism in human radicular pain, and suggest that therapies targeting immune cell activation may be beneficial for chronic pain patients.

Keywords: PET imaging, Sciatica, Integrated PET/MR, Immunoactivation

1. Introduction

Chronic pain is a widespread public health issue, and its prevalence is enormous.[32,41] Unfortunately, despite its great clinical and socioeconomic significance, our understanding of the pathophysiological mechanisms of chronic pain remains incomplete. As a result, currently available treatments (eg, opioids) are unsatisfactory, as they are inefficacious in many patients, and are characterized by numerous side effects including abuse/misuse.

Substantial preclinical evidence has increased recognition of neuroimmune responses at multiple levels of the nervous system as an important contributor to the pathogenesis of persistent pain, including macrophage activation in the dorsal root ganglia (DRG[22,23]), and activation of microglia and/or astrocytes in the spinal cord[10,15,19,29,37,43,48] and brain.[24,42] Because activated macrophages and glial cells produce inflammatory mediators that activate or sensitize nociceptive neurons, the pharmacological inhibition of these cells can significantly reduce nocifensive behaviors in animals.[14,23,30,34,47] As such, the modulation of neuroimmune responses may represent a promising therapeutic strategy for pain disorders.

Among chronic pain disorders, lumbar radiculopathy is one of the most common. It presents clinically as low back pain radiating along the lower extremity (ie, sciatica) along the dermatomes innervated by the affected spinal nerve roots. Lumbar radiculopathy can be caused by multiple etiologies including disk herniation, radiculitis, and lumbar spinal stenosis.[6] Despite the wealth of preclinical information, and knowledge that inflammation is associated with the initial acute phase of lumbar radicular pain,[39] the role of neuroinflammation in chronic lumbar radiculopathy remains unknown. Clinically, the presumption of an inflammatory component to the pathophysiology of chronic

Sponsorships or competing interests that may be relevant to content are disclosed at the end of this article.

M. L. Loggia and Y. Zhang are co-senior authors and contributed equally.

[a] Department of Radiology, A. A. Martinos Center for Biomedical Imaging, Massachusetts General Hospital, Harvard Medical School, Boston, MA, USA, [b] Department of Radiology, Gordon Center for Medical Imaging, Massachusetts General Hospital, Harvard Medical School, Boston, MA, USA, [c] Department of Anesthesia, Critical Care and Pain Medicine, Massachusetts General Hospital, Harvard Medical School, Boston, MA, USA, [d] Department of Radiology, Logan University, Chesterfield, MO, USA, [e] Medical Imaging Centre of Southwest Finland, Department of Diagnostic Radiology, Turku University Hospital, Turku, Finland, [f] Department of Nuclear Medicine and Molecular Imaging, University of Groningen, University Medical Center Groningen, Groningen, Netherlands, [g] Department of Electrical Engineering, Institute of Biomedical Engineering, Polytechnique Montreal, Montreal, QC, Canada, [h] Functional Neuroimaging Unit, CRIUGM, Université de Montréal, Montreal, QC, Canada, [i] Department of Anesthesia, Critical Care and Pain Medicine, Massachusetts General Hospital, Harvard Medical School, Boston, MA, USA

**Corresponding author. Address: MGH Center for Pain Management, Department of Anesthesia, Critical Care and Pain Medicine, Massachusetts General Hospital, Harvard Medical School, 15 Parkman Street, Boston, MA 02114, USA. Tel.: (617) 643-9308. E-mail address: yzhang20@partners.org (Y. Zhang).*

PAIN 0 (2018) 1–10

http://dx.doi.org/10.1097/j.pain.0000000000001171

sciatica, and specifically at the level of the nerve roots, provides a rationale for using anti-inflammatory epidural steroid injections (ESIs) as a treatment strategy for this disorder. However, this treatment demonstrates varying success,[11] suggesting the presence of persistent nerve root inflammation in some patients, but not in others. Moreover, a recent study showed that a brief course of treatment with minocycline, which is thought to reduce central neuroinflammation, leads to some reductions in lumbar radicular pain,[46] suggesting that glial modulation might be a viable treatment for at least some patients, as predicted by animal studies.[19,24,31,38,45] The development of clinical tests capable of detecting spinal nerve root as well as central neuroinflammation would have important clinical implications, including the possibility to guide patient selection for anti-inflammatory therapy targeting the peripheral (eg, ESIs) or the central nervous system (CNS) (eg, glial modulators).

Here, we used simultaneous positron emission tomography/magnetic resonance (PET/MR) imaging and the radioligand [^{11}C]PBR28, which binds to the inflammatory marker 18 kDa translocator protein (TSPO; formerly known as the peripheral benzodiazepine receptor),[2,25,26,48] to test the hypothesis that lumbar radiculopathy is associated with immunoactivation at the level of both the intervertebral foramina (ie, neuroforamina, which include dorsal root ganglion and nerve roots) and spinal cord. Furthermore, we hypothesized that patients demonstrating neuroforaminal inflammation would benefit most from an anti-inflammatory procedure targeting the neuroforamen, that is, an ESI.

2. Methods

2.1. Study design

This cross-sectional study was conducted at the Athinoula A. Martinos Center for Biomedical Imaging and the Translational Pain Research Center at Massachusetts General Hospital, Boston, MA. The protocol was approved by the Institutional Review Board and the Radioactive Drug Research Committee. The study was registered before subject recruitment at www.clinicaltrials.gov (Clinical Trials ID: NCT02130271). The manuscript is written in accordance with the STROBE checklist for observational studies.

2.2. Subjects

Between April 2014 and May 2016, we contacted 309 subjects. Of those contacted, we conducted phone screens on 110 subjects. Nineteen subjects with chronic lower extremity radicular pain lasting at least 3 months and 10 healthy control subjects underwent study procedures. Control subjects were recruited through advertising using flyers and printed announcements posted both within the Massachusetts General Hospital community and from the community at large, and pain patients were recruited using the abovementioned methods and through pools of pain patients under treatment at the Massachusetts General Hospital Center for Pain Medicine. Inclusion criteria for patients were: age between 18 and 75, diagnosis of lower extremity radicular pain with characteristic radiating pain in dermatomal distribution extending below the knee, and ongoing pain intensity of 4 or greater using the visual analog scale during the week before enrollment. L4 dermatome pain was defined as presenting in the anterior thigh and medial leg. L5 and S1 dermatome pain was defined as presenting in the posterolateral thigh and leg. All subjects were excluded for: recent hospitalization for a major psychiatric disorder, endorsing or testing positive for illicit drug use, chronic corticosteroid therapy, chronic opioid therapy, regular use of nonsteroidal anti-inflammatory drugs, recent lumbar ESIs (within 8 weeks), active cardiopulmonary disease, hepatic or renal insufficiency, any known inflammatory disease (eg, inflammatory bowel disease), or any contraindications for PET or MR scanning (eg, pregnancy, claustrophobia, ferromagnetic implants, etc.). Study procedures were fully explained to all subjects, and all subjects read and signed an informed consent document.

2.3. Screening visit

Each patient underwent a characterization session, which included a brief medical history and clinical examination by a board-certified pain management specialist (Y.Z. or S.A.). The clinical examination determined the laterality of radicular pain (left or right leg), the dermatome affected, duration of pain (years), current subjective pain level (visual analog scale, anchored with 0 = "no pain" and 10 = "the most intense pain imaginable"), and response to previous ESIs (if any). Blood was collected to genotype subjects for the Ala147Thr *TSPO* polymorphism which is known to affect binding affinity for [^{11}C]PBR28.[21,35] Low-affinity binders (Thr/Thr; N = 2) were excluded from all analyses, whereas high-affinity (Ala/Ala) or mixed-affinity binders (MABs) (Ala/Thr) were included. Urine was collected to test and exclude for recent illicit drug use.

2.4. Positron emission tomography/magnetic resonance imaging

All simultaneous PET/MR imaging was performed on a 3T Siemens Biograph mMR system (Siemens Medical Solutions USA, Inc, Malvern, PA) with the radioligand [^{11}C]PBR28. [^{11}C]PBR28 binds to TSPO, a protein mostly expressed in the outer mitochondrial membrane. Although TSPO is constitutively expressed by various cell types,[7] it is commonly used as a marker of CNS inflammation because it is expressed at low levels in the healthy CNS, and it is dramatically upregulated in activated microglia and/or astrocytes in the context of neuroinflammation, including in response to spinal nerve injury.[2,25,26,48] Additionally, TSPO is upregulated in activated macrophages,[22] and therefore can also be used as a marker of peripheral inflammation. [^{11}C]PBR28 was produced in-house using a procedure modified from the literature.[18]

2.5. Magnetic resonance imaging–related details

Magnetic resonance imaging data acquisition was performed using the body coil for transmit and a combination of the 4-channel body matrix coils and the spine array matrix for receive. Imaging focused on both the lumbar neuroforamina and lower thoracic spinal column. Anatomical images were collected using a combination of T1- and T2-weighted sequences. A T1-weighted (T1W) 2-point Dixon 3D volumetric interpolated breath-hold examination sequence was acquired with the following parameters: parallel acquisition technique GRAPPA factor 2, repetition time (TR) = 3.60 seconds, echo time 1 (TE1) = 1.23 ms, TE2 = 2.46 ms, flip angle (FA) = 10°, slice thickness = 3.12 mm, and in-plane resolution = 4.1 × 2.6 mm. The resulting images were segmented in-line to create a mu-map for MR-based attenuation correction of the PET data. Magnetic resonance–based attenuation correction scans were acquired immediately before initiation of PET scans. A high-resolution T1W

axial anatomical turbo spin echo sequence was acquired with the following parameters: TR = 2.69 seconds, TE = 12ms, FA = 170°, matrix size = 256 × 179, slice thickness = 2 mm, number of slices = 46, and in-plane resolution = 1.0 × 0.7 mm. This sequence was used for manual tracing of neuroforaminal regions of interest (ROIs).

A T1W axial in-opposed phase gradient recoil echo sequence was acquired with the following parameters: TR = 2.63 seconds, TE = 3.83 ms, FA = 65°, matrix size = 260 × 150, slice thickness = 2 mm, number of slices = 76, and in-plane resolution = 1.48 × 1.48 mm. The field of view (FOV) was centered at the L4-L5 intervertebral disk. This sequence was used for visualization of overlaid PET signal.

A high-resolution T2-weighted sagittal anatomical turbo spin echo sequence was acquired with the following parameters: TR = 3.38 seconds, TE = 109ms, FA = 150°, matrix size = 265 × 384, slice thickness = 2 mm, number of slices = 30, and in-plane resolution = 0.9 × 0.6 mm, with the FOV centered at the L4-L5 intervertebral disk. This was used for registration of PET data and extracting PET signal.

2.6. Positron emission tomography acquisition

All subjects participated in a 90-minute dynamic acquisition, initiated with IV administration of [^{11}C]PBR28. Injected radioactivity (mean ± SD) was 392.6 ± 60 MBq for patients and 393.3 ± 57 MBq for controls (P = 0.97). After the 90-minute lumbar neuroforamina PET scan, in a subset of willing participants (N = 9 patients and N = 9 controls), the PET FOV was shifted to image the lower thoracic spinal column, and an additional 20 minutes of dynamic PET data were then acquired in listmode format.

2.7. Data processing

For the neuroforaminal scan, a 30-minute static image was reconstructed from the 60 to 90 minutes' postinjection period. Images were reconstructed using 3D-OSEM and a 4-mm FWHM Gaussian kernel filter. Attenuation correction was performed using the MR-based attenuation correction–based mu-maps expanded using PET emission data and the maximum likelihood reconstruction of attenuation and activity. Positron emission tomography images were converted from Bq/mL to standardized uptake value (SUV) maps by dividing all voxels by injected dose/body weight. Standardized uptake value maps and high-resolution T1W images were imported into Osirix version 3.9.4 (http://www.osirix-viewer.com) for defining ROIs and extracting SUV. Fused PET/MR images were visually inspected to ensure the absence of motion artifacts. Magnetic resonance and PET images were well aligned for most subjects, but several patient and control PET scans required registration to MR data, which was manually performed using Osirix. On the T1W image, ROIs were manually traced on the left and right neuroforamina at the intervertebral level of L3-L4, L4-L5, and L5-S1, the levels affected in the majority of lumbar radiculopathy patients. Neuroforamina definition was determined by anatomical boundaries: anterior—intervertebral disk/vertebrae; medial—thecal sac; posterior—apophyseal joint; and lateral—psoas muscle. The structures contained in this area included the exiting spinal nerve roots, the corresponding DRG, and a cross section of the nerve root traversing to the lower adjacent level (**Fig. 1A**). Determination of neuroforaminal ROIs was performed by a trained examiner and confirmed by an expert radiologist. Average neuroforaminal SUV was extracted for each intervertebral level on axial sections, targeting the regions directly adjacent to intervertebral disks to minimize signal bleed from vertebrae. In addition, one subject's data were unusable due to attenuation artifacts and the inability to anatomically delineate the ROI, caused by a previous spinal fusion. There was no major pathological change impairing visualization of any neuroforaminal or spinal cord region for any other subjects. Standardized uptake value ratio (SUVR) was calculated in patients by taking the ratio of SUV in target ROI (side ipsilateral to pain) to SUV in reference ROI (side contralateral to pain). In controls, SUVR was computed by taking the ratio of left to right SUV.

For the thoracic spinal PET data, a 20-minute static image was reconstructed from 90 to 110 minutes post-injection. Images were reconstructed and converted to SUV maps using the same procedure as for neuroforaminal data. Processing of the spinal cord images was performed with the recently developed Spinal Cord Toolbox (SCT).[13] Spinal Cord Toolbox

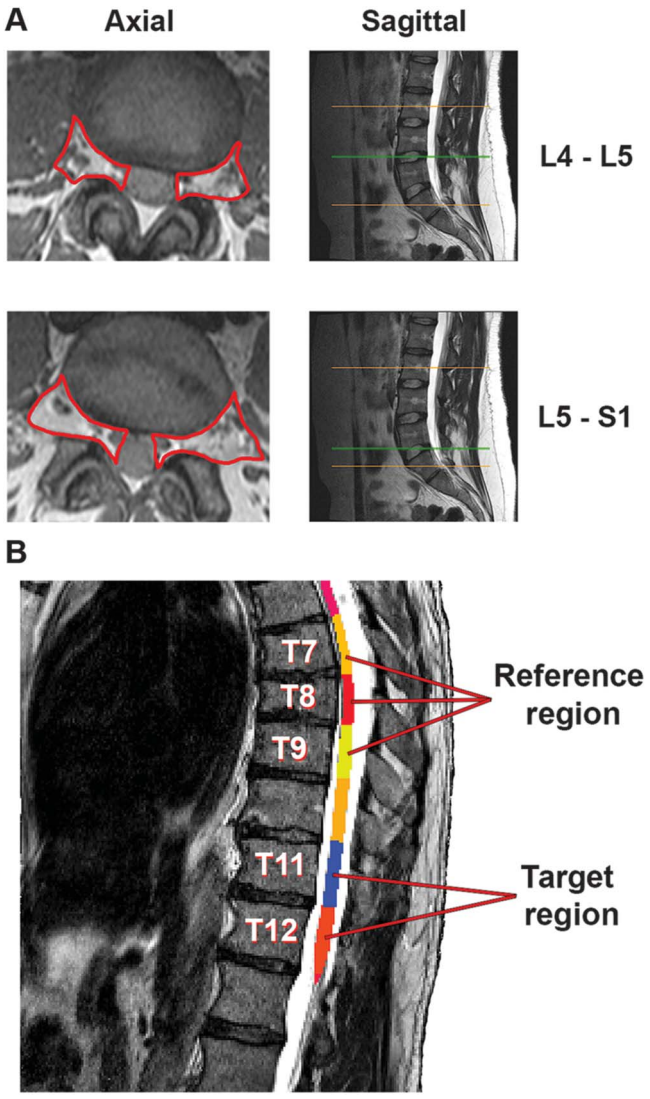

Figure 1. Visualization of spinal root and cord ROI placement. (A) Neuroforamina ROI labels. Right: Sagittal T2W images are shown to visualize the caudal/rostral level of ROI placement. Left: ROIs were manually drawn on the high-resolution T1W axial TSE sequence at the L3-L4, L4-L5, and L5-S1 levels (the latter 2 are pictured here). (B) Spinal cord ROI labels. Cord segments contained in T7, T8, and T9 served as the reference region. Segments contained in T11 and T12 were target regions because this level of spinal cord receives nociceptive input from L4, L5, and S1 spinal roots. ROI, region of interest; T1W, T1-weighted; T2W, T2-weighted; TSE, turbo spin echo.

Table 1

Characteristics of pain patients enrolled in the study.

Root analysis	Radicular pain patients (N = 16)	Healthy controls (N = 10)
Age (y)	51.2 ± 14	43.1 ± 19
Sex	6 F and 10 M	4 F and 6 M
TSPO genotype	6 HAB and 10 MAB	4 HAB and 6 MAB
Injected dose (mCi)	10.6 ± 1.6	11.0 ± 0.6
BMI	25.7 ± 2.8	27.1 ± 5.1
Location of pain (dermatome)	1—L4; 15—L5 and S1	N/A
Location of pain (Laterality)	8—Left, 8—Right	N/A
Pain intensity (visual analog score)	6.2 ± 1.5	N/A
Pain duration (y)	5.6 ± 4.2	N/A
Spinal cord analysis	**Radicular pain patients (N = 9)**	**Healthy controls (N = 9)**
Age (y)	50.2 ± 9.0	42.4 ± 20
Sex	2 F and 7 M	3 F and 6 M
TSPO genotype	2 HAB and 7 MAB	4 HAB and 5 MAB
Injected dose (mCi)	10.5 ± 1.7	10.5 ± 2.1
BMI	24.1 ± 3.6	26.8 ± 5.2
Pain intensity (visual analog score)	6.17 ± 1.7	N/A
Pain duration (y)	3.94 ± 2.2	N/A

Patient demographics and clinical characteristics. All continuous values are shown in mean ± SD. To differentiate subject subsamples from the spinal root and cord analyses, characteristics from each of the patient and control subgroups are displayed separately here. There were no significant group differences in any subject variables displayed here, for either spinal root or spinal cord analyses ($P > 0.21$).
BMI, body mass index; HAB, high-affinity binder; F; female, M, male; MAB, mixed-affinity binder; TSPO, translocator protein.

enabled automated segmentation of whole spinal cord and labeling of vertebral levels from the high-resolution T2-weighted image. As for the root data, MR and PET images of the spinal cord were well aligned for most subjects, but in a few subjects required coregistration, which was performed using SCT. The spinal cord contained in T11-T12 vertebrae was chosen as a target region (**Fig. 1B**), as the cord below and including T11 contains the lower lumbar/upper sacral spinal segments that receive nociceptive input from the sciatic nerve,[40] and T11-T12 was present in all scanned participants (some participants had spinal cord termination above L1 due to natural interindividual variability). In 1 patient and 2 controls, the full extent of the cord contained in T12 was not present in the image; for these subjects, the partial cord contained in T12 was included in the target region. Spinal cord contained in T7-T9 vertebrae was selected as a reference region, as these spinal segments are anatomically distant from those processing nociceptive input from the dermatomes affected in lumbar radiculopathy (**Fig. 1B**). Standardized uptake value was extracted from target and reference cord regions using the SCT. Standardized uptake value ratio was calculated by taking the ratio of target ROI (cord contained in T11-T12) SUV to reference ROI (cord contained in T7-T9) SUV.

2.8. Epidural steroid injections

Lumbar ESIs were provided by patients' own treating physicians as part of their medical care. All ESIs were performed conforming to current standard of care with a fluoroscopic guided, paramedian interlaminar approach on the side of pain symptoms and at the level of the involved nerve root (L4-L5 level for L4 dermatomal pain and L5-S1 level of L5 or S1 dermatomal pain). A total volume of 4 mL (2 mL of 40 mg/mL triamcinolone and 2 mL of 0.25% bupivacaine) was administered after fluoroscopic confirmation of contrast dye spread in the epidural space. All injections were considered successful by their treating physicians and confirmed by contrast spread under fluoroscopy. Seven patients received ESIs after the PET/MR scan. Six of them received ESI treatments within 2 months after the scan. One subject received ESI treatment 8 months after the scan as the subject had medical insurance coverage in the interim. Two patients received ESIs 3 to 6 months before enrollment in the study but had no further ESIs up to 2 years after the scan. Therefore, we included these 2 patients with retrospective ESI treatment in the ESI response analysis. Subjective perception of percentage pain relief was documented at their follow-up visits 4 weeks after the ESI treatment. For the 2 patients who received ESIs before enrollment, patients reported response to the previous ESI was documented at time of enrollment. Positive ESI response was defined as >30% pain relief and negative response was defined as <30% pain relief. The positive responders (N = 5) reported 90 ± 11% relief from ESI and all negative responders (N = 4) reported 0% relief from ESI.

2.9. Statistical analysis

Descriptive statistics were summarized for both continuous and categorical variables. Continuous variables were compared with *t* tests. Based on the assumption that there should be no difference in PET signal between target and reference regions within healthy controls, we created an a priori derived grouping factor ("region"): "target" region in patients (neuroforamen analysis—neuroforamen ipsilateral to symptomatic leg in the affected dermatome; spinal cord analysis—cord contained in T11-T12 vertebrae), "reference" region in patients (neuroforamen analysis—neuroforamen contralateral to symptomatic leg in the affected dermatome; spinal cord analysis—cord contained in

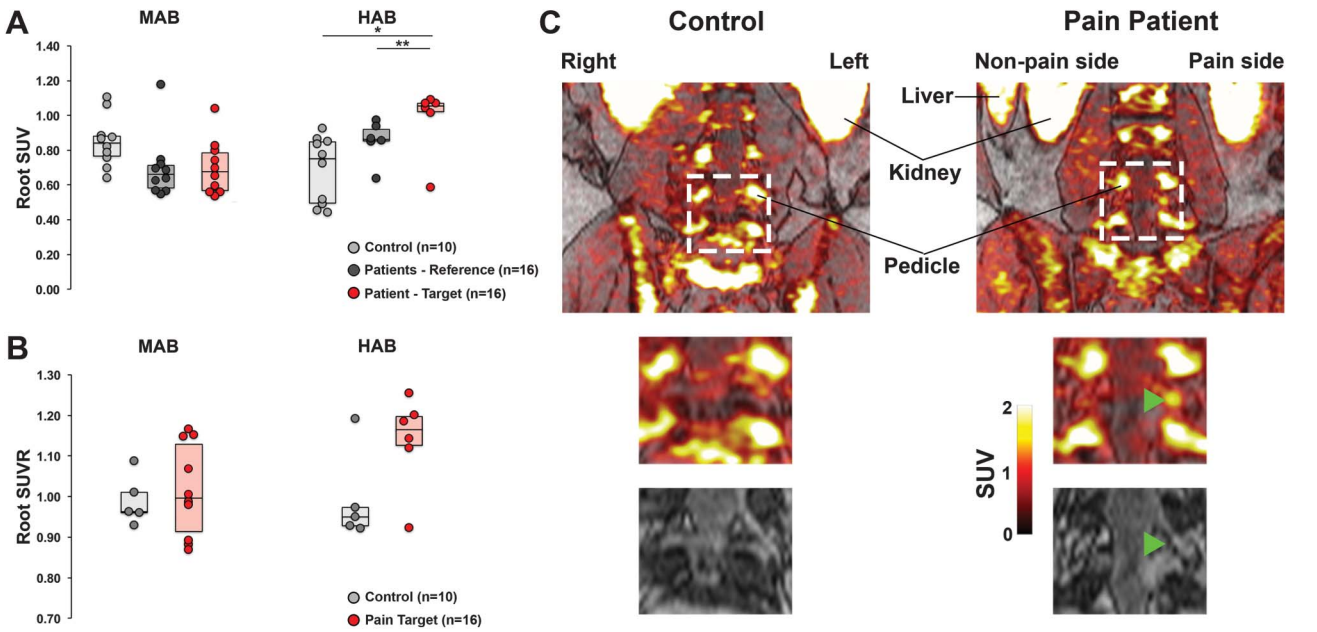

Figure 2. Regional differences in spinal root [^{11}C]PBR28 signal. (A) A linear mixed-effects model showed that high-affinity binding patients had elevated tracer uptake on the side ipsilateral to pain, relative to the side contralateral to pain and to uptake in healthy controls. Boxes represent 25% to 75% interquartile range, and horizontal line represents the median. $^{*}t_{(27.4)} = -3.09$, $P = 0.016$; $^{**}t_{(26)} = -4.10$, $P < 0.001$, corrected. (B) Between-group comparison of spinal root SUVR (patients—target divided by reference neuroforamina SUV and controls—left divided by right neuroforamina SUV). Statistical results from a linear regression analysis are shown in Table 3. (C) Individual lumbar PET/MR scans from 2 subjects, matched for age (control—49; patient—47), sex (M), and *TSPO* genotype (HAB). On the right (pain patient), focal elevation of [^{11}C]PBR28 uptake in the L4-L5 neuroforamen ipsilateral to the side of pain is highlighted by green arrowheads, compared with unaffected, contralateral side. This can be compared with the absence of neuroforaminal signal in the control subject's scan (left). The dashed boxes in the top panels are enlarged in the middle (PET overlaid on MR) and bottom (MR only) panels. Note: the coronal sections are shown only for display purposes; all data were extracted from axial slices. HAB, high-affinity binder; MAB, mixed-affinity binder; MR, magnetic resonance; PET, positron emission tomography; SUV, standardized uptake value; SUVR, standardized uptake value ratio; TSPO, translocator protein.

T7-T9), and healthy control region (neuroforamen analysis—left and right L5-S1 neuroforamen, as this was the affected dermatome in all but one pain patients; spinal cord analysis—cord contained in T7-T9 and T11-T12). To account for repeated measures within an individual, we used a subject-level random intercept in mixed-effects models while assessing the fixed effect regional differences in [^{11}C]PBR28 uptake in neuroforamen and spinal cord, controlling for *TSPO* genotype (high- or mixed-affinity binding status). Reference region in patients and mixed-affinity binding were included as reference terms within the mixed model.

We hypothesized that genotype would differentially moderate regional differences in [^{11}C]PBR28 uptake; so, we used analysis of variance F statistics to test whether adding a region × genotype interaction term would significantly increase the model fit from a model not including the interaction, as determined by Akaike information criterion.[1] If it was determined that addition of a region × genotype interaction improved the model fit, it was included in the model. Bonferroni-adjusted pairwise post hoc comparisons were performed across regions (if applicable, at each level of genotype). Two initial post hoc

Table 2

Linear mixed model statistics for spinal root SUV analysis.

	Estimate	Std. error	*df*	*t*-value	*P*	2.5% CI	97.5% CI
Intercept	0.697	0.05	29.1	13.942	<0.0001	0.595	0.798
			Region				
Patients—reference				Reference			
Healthy controls	0.153	0.085	27.0	1.804	0.082	−0.019	0.326
Patients—target	0.004	0.024	26.0	0.171	0.866	−0.044	0.052
			Genotype				
MAB				Reference			
HAB	0.157	0.082	29.1	1.926	0.064	−0.008	0.323
			Region × genotype				
Patients—reference × HAB				Reference			
Healthy controls × HAB	−0.319	0.127	27.2	−2.515	0.018	−0.577	−0.061
Patients—target × HAB	0.121	0.039	26.0	3.133	0.004	0.043	0.2

We included a region × genotype interaction term in the primary model that was retained in the final model as the addition of the interaction term was found to significantly improve the model fit. Bonferroni adjusted post hoc comparisons compared mean outcomes at each level of genotype by region. Planned pairwise comparisons were between patient target and patient reference regions, and between patient target and healthy control regions. Reference side in patients for region and mixed-affinity binding for genotype were used as reference terms within the model. The mixed-model showed significant interactions between *TSPO* genotype and neuroforamen SUV. Post hoc testing revealed that this interaction was driven by significant increases in target SUV relative to reference SUV within patients as well as healthy control SUV in high-affinity binding individuals.
CI, confidence interval; HAB, high-affinity binder; MAB, mixed-affinity binder; SUV, standardized uptake value.

Table 3

Linear regression results from spinal root standardized uptake value ratio analysis.

	Estimate	Std. error	*t*-value	*P*
Intercept	0.990	0.048	20.7	1×10^{-14}
Group	0.025	0.059	0.428	0.673
Genotype	0.003	0.068	0.041	0.968
Group × genotype interaction	0.120	0.087	1.375	0.183

This analysis did not replicate the significant differences in spinal root [^{11}C]PBR28 uptake seen with the regional linear mixed model ($F_{(3,22)} = 2.52$, $P = 0.08$, $R^2 = 0.26$; Fig. 2A).

comparisons were planned, one comparing target region to reference region in patients, and one comparing target region in patients to healthy control regions. Supplementary linear regressions were also conducted to assess the effect of region and genotype on SUVR for both the spinal root and spinal cord analyses. Correlations between 2 continuous variables were estimated using linear regression. All statistical tests were 2-tailed with alpha set to 0.05. All analyses were performed using R statistical computing software (R, version 3.2.2; R Foundation for Statistical Computing, Vienna, Austria; Rstudio Version 1.0, Boston, MA).

3. Results

3.1. Subjects

Twenty-six subjects (patients, n = 16 and controls, n = 10) and 18 subjects (patients, n = 9 and controls, n = 9) were included in the spinal root and spinal cord analyses, respectively. Patient and control characteristics for both analyses are listed separately in **Table 1**. There were no significant group differences in age, sex, *TSPO* genotype, injected dose, or BMI for either analysis ($P > 0.21$).

3.2. Neuroforaminal immune activation in chronic lumbar radiculopathy

Using a mixed-effects model, [^{11}C]PBR28 signal was compared across 3 anatomically-defined regions (grouping factor "region"): neuroforamen corresponding to pain symptoms in 16 patients (ie, "target" region), neuroforamen contralateral to target region in patients (ie, within-subject "reference" region), and corresponding neuroforamina in 10 healthy controls. We found that addition of a region x genotype interaction to the model significantly improved the fit ($F_{(48,46)} = 8.15$, $P = 0.0009$, analysis of variance; Akaike information criterion = −68.6), and thus, was included in the final model. The model revealed that, for high-affinity binders only, the "target" neuroforaminal PET signal in patients was significantly elevated relative to both the signal from the "reference" side in the same individuals ($t_{(26)} = -4.10$, $P < 0.001$, corrected) as well as signal in healthy controls ($t_{(27.4)} = -3.09$, $P = 0.016$, corrected; **Figure 2A and C**, **Table 2**). In MABs, "target" PET signal was not significantly different than "reference" side in the same patients ($t_{(26)} = -0.17$, $P = 0.99$, corrected) or in healthy controls ($t_{(27)} = 1.76$, $P = 0.36$, corrected; **Figure 2A** and **Table 2**). The absence of a significant regional effect in the MABs is likely due to the fact that a lower proportion of the PET signal in these participants reflects specific binding to TSPO.[35] See **Figure 2B** and **Table 3** for a complementary linear regression analysis using SUVR ($F_{(3,22)} = 2.52$, $P = 0.08$, $R^2 = 0.26$).

3.3. Association between neuroforaminal [^{11}C]PBR28 signal and epidural steroid injection–induced pain relief

A subset of patients (N = 7) were treated with fluoroscopy-guided ESIs one week to several months after the imaging session. Two additional patients received ESIs more than 2 months before scanning. Five patients (4 prospective and 1 retrospective ESI) reported 90 ± 11% relief from ESI (positive responders) and 4 patients (3 prospective and 1 retrospective ESI) reported 0% relief from ESI (negative responders). We found that a positive response to ESI was observed only in patients with a ratio of target-to-reference SUV greater than 1 (ie, target SUV > reference SUV; **Fig. 3**). That is, a higher level of [^{11}C]PBR28 signal in the neuroforamen ipsilateral to pain, compared with the contralateral side, was associated with a positive response to ESI.

3.4. Spinal cord neuroinflammation in chronic lumbar radiculopathy

To determine whether radicular pain was also associated with spinal cord inflammation (ie, glial activation), [^{11}C]PBR28 cord data were acquired in a subset of patients (N = 9) and controls (N = 9). Data were assessed with a mixed-effects model between

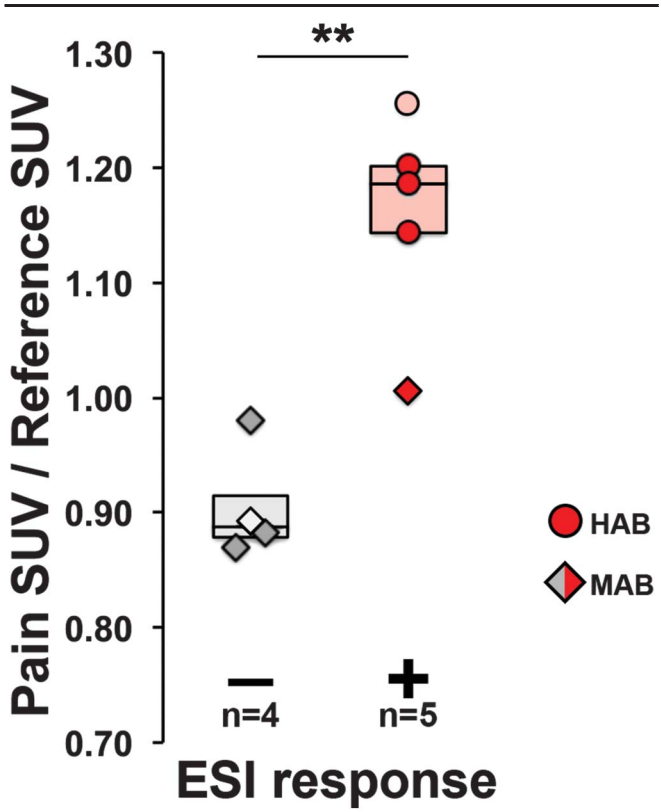

Figure 3. Comparison between spinal root laterality (target SUV/reference SUV) in ESI nonresponders (n = 4; mean relief 0 ± 0%) and ESI responders (n = 5; mean relief 90 ± 11%). Epidural steroid injection responders have a ratio of pain SUV to reference SUV greater than 1, indicating that increased lateral uptake in roots ipsilateral to pain is associated with a positive response to ESI. This is true both when using prospective data alone (ie, patients receiving the ESI after the PET/MR scan) and also when including 2 retrospective subjects, $^{**}t_{(4.99)} = -3.94$, $P = 0.011$; and $t_{(6.27)} = -5.13$, $P = 0.002$, respectively, Welch 2-sample *t* test. Light gray and light red identify a retrospectively-treated ESI nonresponder and a responder, respectively. ESI, epidural steroid injection; HAB, high-affinity binder; MAB, mixed-affinity binder; MR, magnetic resonance; PET, positron emission tomography; SUV, standardized uptake value.

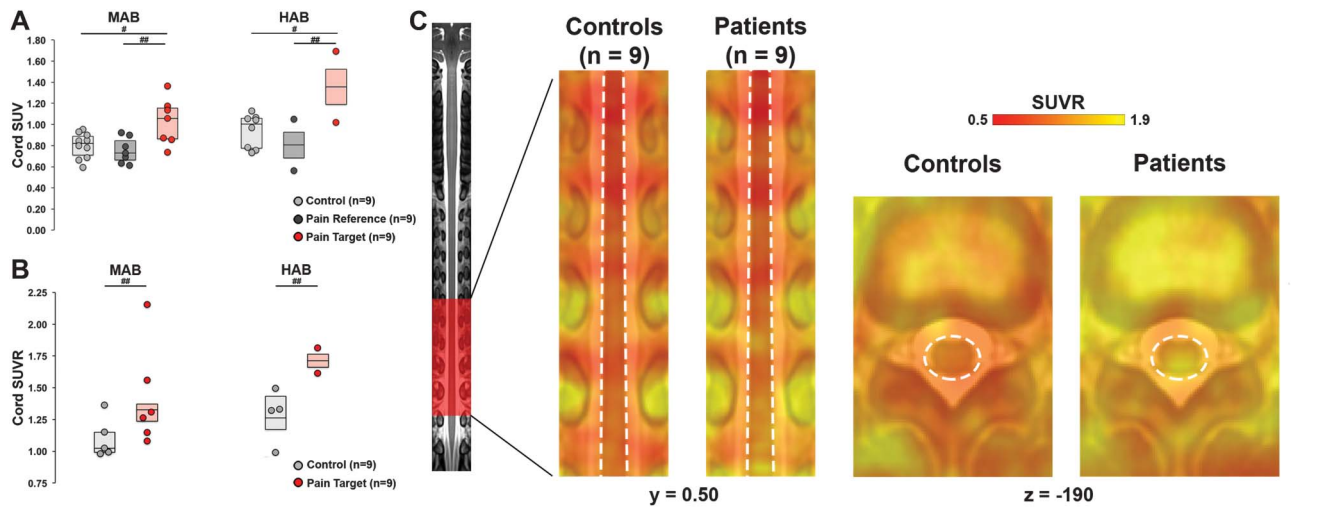

Figure 4. Regional comparison of spinal cord [^{11}C]PBR28 uptake. (A) A linear mixed-effects model showed that patients had elevated SUV in spinal cord contained in T11-T12 vertebrae, relative to spinal cord contained in T7-T9 vertebrae in patients and to uptake in healthy controls. Boxes represent 25% to 75% interquartile range, and horizontal line represents the median. Although a genotype interaction term was not retained in this statistical model as it did not improve model fit, data from HAB and MAB subjects are presented separately here for illustrative purposes, and for consistency with Figure 2A. #Differences between target signal in patients and signal in healthy controls (main effect, irrespective of genotype), $t_{(26.9)} = -3.6$, $P = 0.002$ (corrected); ##Differences between target and reference in patients (irrespective of genotype), $t_{(18)} = -4.82$, $P < 0.001$ (corrected). (B) Between-group comparisons of spinal cord SUVR (SUV from cord contained in T11-T12 divided by SUV from cord contained in T7-T9). See Table 5 for the results from a linear regression analysis. Although a genotype interaction term was not retained in this statistical model, data from HAB and MAB subjects here are presented separately for illustrative purposes, and for consistency with Figure 2B. ##Differences between patient and control SUVR (main effect, irrespective of genotype) at $P = 0.024$ (Table 5). (C) Mean spinal cord PET SUVR images for both controls and patients. Coronal and axial slices in the middle and right of the panel show [^{11}C]PBR28 data overlaid on the SCT T2 template. White dashed lines denote the borders of the spinal cord. A full-length image of the SCT T2 template on the left displays the spinal region common to all subjects (red overlay). The images shown here in SCT template space are for visualization purposes only; all data were extracted from images in subject space. HAB, high-affinity binder; MAB, mixed-affinity binder; PET, positron emission tomography; SCT, Spinal Cord Toolbox; SUV, standardized uptake value; SUVR, standardized uptake value ratio.

3 regions: PET signal (SUV) from patients' cord contained in T11-T12 spinal segments ("target" region, which contains the spinal cord representations of the sciatic nerve), patients' T7-T9 signal (within-subject "reference" region), and the corresponding regions in controls. We found that target signal was significantly greater than both reference signal in patients as well as signal in healthy controls ($t_{(18)} = -4.82$, $P < 0.001$; $t_{(26.9)} = -3.6$, $P = 0.002$, respectively, corrected; **Figure 4A** and **Table 4**). See **Figure 4B** and **Table 5** for a complementary-related SUVR analysis ($F_{(2,15)} = 3.85$, $P = 0.04$, $R^2 = 0.34$). We did not observe significant associations between neuroforaminal and cord SUVR ($F_{(1,6)} = 0.21$, $P = 0.66$, $R^2 = 0.03$; **Figure 5**), between ESI response and spinal cord uptake ($P = 0.78$), or between central or peripheral PET metrics and pain ratings ($P = 0.23$ and 0.13, respectively).

4. Discussion

We present here results supporting the occurrence of spinal neuroinflammation in patients with chronic radicular pain. Specifically, we show that patients demonstrate elevated TSPO levels, a putative marker of immune activation,[2,22,25,26,48] in both nerve roots (ipsilateral to the symptomatic leg) and in the spinal cord (in spinal segments known to process sensory information from the legs). These findings, which extend and complement our earlier observations that TSPO levels are elevated in the brain of chronic low back pain patients,[27] support the role of immunoactivation of the nerve roots as well as glial activation in the CNS as key components of the pathophysiology of chronic radicular pain. This is in line with a large body of preclinical data demonstrating neuroimmune activation as a result of peripheral nerve injury, both in the peripheral nervous system (eg, DRG, nerve roots[22,23]) and

Table 4

Linear mixed model statistics for spinal cord SUV analysis.

	Estimate	Std. error	*df*	*t*-value	*P*	2.5% CI	97.5% CI
Intercept	0.73	0.06	32.4	12.128	<0.0001	0.609	0.853
Region							
Patients—reference					Reference		
Healthy controls	0.062	0.076	26.9	0.812	0.424	−0.093	0.216
Patients—target	0.335	0.07	18.0	4.815	<0.0001	−2.238	0.479
Genotype							
MAB					Reference		
HAB	0.162	0.072	18.0	2.254	0.037	0.066	0.261

A region × genotype interaction term was not retained in the final model as it was found to not significantly improve the model fit. Bonferroni adjusted pairwise post hoc comparisons were proposed to compare mean outcomes at each region. Standardized uptake value in spinal cord contained in T7-T9 vertebrae for region and mixed-affinity binding for genotype were used as reference terms within the model. There was a significant difference between reference T7-T9 SUV in patients and SUV in cord contained in T11-T12 in patients. There was also a significant effect of genotype.
CI, confidence interval; HAB, high-affinity binder; MAB, mixed-affinity binder; SUV, standardized uptake value.

Table 5

Linear regression results from spinal cord SUVR analysis.

	Estimate	Std. error	*t*-value	*P*
Intercept	1.08	0.110	9.82	1×10^{-6}
Group	0.331	0.131	2.52	0.024
Genotype	0.241	0.139	1.73	0.104

The analysis replicated significant group differences in spinal cord SUVR (T11-T12 cord SUV normalized by T7-T9 cord SUV) between patient and control groups that were seen in SUV regional analysis ($F_{(2,15)} = 3.85$, $P = 0.04$, $R^2 = 0.34$; Fig. 4A).
SUVR, standardized uptake value ratio.

CNS, including spinal cord[10,14,15,34,37,43,48] and brain.[24,42] Previous studies have documented elevations in inflammatory mediators (eg, proinflammation interleukins, prostaglandins, tumor necrosis factor-α, etc.) occurring in spinal tissue and CSF in individuals with disk disease, including herniation and degeneration.[39,49] This evidence indirectly suggests the involvement of neuroimmune modulation in these patients because neuroimmune cells produce many of these molecules when activated during inflammation. More recently, studies using [^{18}F]FDG PET to assess metabolic activity showed increased binding in the spinal cord and compressed nerve roots of radicular pain patients[9,50] and in healthy aging subjects,[4] that was suggested to be related to inflammatory activity. Although these studies are informative, the present experiment provides more direct insight into the role of neuroinflammation in lumbar radiculopathy because it presents, for the first time, in vivo evidence supporting elevated levels of a marker of immune activation.

Our findings suggest that immune responses in both central and peripheral nervous system may represent a promising therapeutic target. In the treatment of chronic sciatica pain, besides targeting spinal nerve roots with ESI as in current clinical practice, central immune activation may also need to be targeted for therapeutic intervention, as suggested by numerous preclinical studies.[14,19,24,30,34,37,43,48] Large-scale studies are warranted to elucidate the relationship between these inflammatory signals and symptoms, as well as their viability as possible therapeutic targets and disease biomarkers. Once a definitive role for neuroinflammation in the pathology of sciatica has been confirmed in large-scale studies, it will be important to investigate surrogate techniques for identifying neuroinflammation that are more economic and do not include ionizing radiation for widespread use in a clinical setting. Integrated PET/MR imaging will likely be instrumental in the development of these surrogate strategies because it allows for a direct evaluation of the association between PET and MRI metrics simultaneously collected.

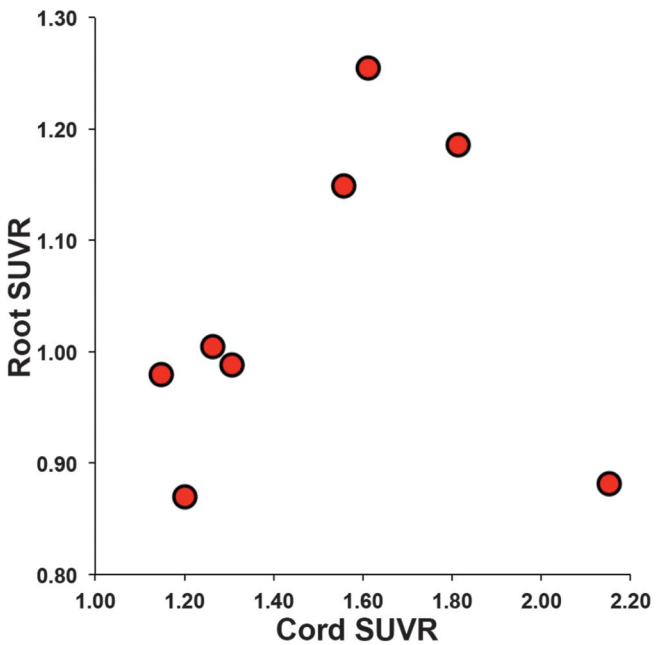

Figure 5. Relationship between spinal root and spinal cord SUVR. The association between spinal root and spinal cord SUVR was not significant with the inclusion of all pain patients for whom both root and spinal cord data were available (n = 8). However, the regression became significant ($F_{(1,5)} = 17.13$, $P = 0.009$, $R^2 = 0.77$) after removal of one subject (bottom right). Notably, this subject did not receive any relief after ESI. ESI, epidural steroid injection; SUVR, standardized uptake value ratio.

In our data, the ratio in [^{11}C]PBR28 signal between target and reference neuroforamen was associated with the response to ESI. These results suggest that variability in the magnitude of neuroforaminal inflammation may explain the large variability in responses to this treatment.[11] With validation in larger samples, our data suggest that preselecting patients based on the presence and/or magnitude of neuroforaminal inflammation might improve overall treatment response. It is important to note, however, that all but one of the patients who were positive responders also possessed a high-affinity binding *TSPO* genotype. Although the effect of the Ala147Thr substitution in the *TSPO* gene on the binding affinity to second generation TSPO ligands is well known, the functional or clinical significance of this polymorphism is not well understood. One recent study did show that high-affinity binding status was associated with higher pain sensitivity in patients with fibromyalgia,[20] suggesting that TSPO may play a role in modulating pain sensitivity, perhaps through its effects on neurosteroid production.[12] However, that association, along with the observations in the current dataset, will need to be validated with larger studies.

4.1. Study limitations

Several additional caveats in this study need to be mentioned. Analysis of PET data with an arterial input function and kinetic modeling is traditionally performed to quantify signal. However, there is a high amount of variability and complications associated with traditional modeling of TSPO PET data.[44] For this reason, SUV and SUVR metrics are being increasingly used in TSPO PET analyses,[3,5,8,16,17,27,28,33,36,51] as we report here.

It is also important to acknowledge that the PET signal from both neuroforaminal and cord ROIs is likely to include partial volume contribution from surrounding tissues (eg, vertebrae), due to the coarse resolution of PET imaging (~4 mm at center of field of view). However, the use of within-subject controls (the asymptomatic neuroforamen and the upper thoracic spinal cord segment) limits the impact of this concern because both target and control regions should be similarly affected. In addition, there were no significant differences in the average PET signal in the vertebrae, or in size of target/reference ROIs ($P > 0.10$, data not shown), giving us further confidence that the contamination from vertebral signal should not have significantly biased our results.

Another limitation of our study includes a relatively small sample size, particularly for the spinal cord data and the longitudinal component evaluating the association between neuroforamen TSPO uptake and ESI treatment response. Thus, further studies are needed to validate and expand on these findings. Additionally, part of the treatment outcome data were collected retrospectively and thus is subject to patient recall bias.

The time between the subjects PET/MRI scan and ESI treatment was not uniform, although this is unlikely to have affected the causality between PET findings and ESI response because all patients had chronic lumbar radicular pain with stable pain symptoms.

Although these caveats necessitate the use of caution when interpreting the results from our study, our preliminary observations are in line with previous preclinical literature supporting a role for neuroimmune activation in the establishment and/or maintenance of persistent pain conditions.

Conflict of interest statement

The authors have no conflict of interest to declare.

The study was supported by the following funding sources: 1R01NS095937-01A1 (M. L. Loggia), 1R21NS087472-01A1 (M. L.L.), NS082548-01A1 (Y.Z. and J.H.), and 5T32EB13180 (T32 supporting D.A.).

Acknowledgments

The authors thank Grae Arabasz, Shirley Hsu, and Regan Butterfield for their help with data acquisition.

Article history:
Received 12 October 2017
Received in revised form 18 January 2018
Accepted 24 January 2018
Available online 5 February 2018

References

[1] Akaike H. Information theory and an extension of the maximum likelihood principle. Breakthroughs in statistics. New York, NY: Springer, 1992. pp. 610–24.
[2] Albrecht DS, Granziera C, Hooker JM, Loggia ML. In vivo imaging of human neuroinflammation. ACS Chem Neurosci 2016;7:470–83.
[3] Albrecht DS, Normandin MD, Shcherbinin S, Wooten DW, Schwarz AJ, Zurcher NR, Barth VN, Guehl NJ, Johnson-Akeju O, Atassi N, Veronese M, Turkheimer F, Hooker JM, Loggia ML. Pseudo-reference regions for glial imaging with 11C-PBR28: investigation in two clinical cohorts. J Nucl Med 2017;59:107–14.
[4] Aliyev A, Saboury B, Kwee TC, Torigian DA, Basu S, Wulff Christensen H, Alavi A. Age-related inflammatory changes in the spine as demonstrated by (18)F-FDG-PET:observation and insight into degenerative spinal changes. Hell J Nucl Med 2012;15:197–201.
[5] Alshikho MJ, Zurcher NR, Loggia ML, Cernasov P, Chonde DB, Izquierdo Garcia D, Yasek JE, Akeju O, Catana C, Rosen BR, Cudkowicz ME, Hooker JM, Atassi N. Glial activation colocalizes with structural abnormalities in amyotrophic lateral sclerosis. Neurology 2016;87: 2554–61.
[6] Benzon H, Rathmell JP, Wu CL, Turk DC, Argoff CE. Raj's practical management of pain. Philadelphia, PA: Elsevier Health Sciences, 2008.
[7] Bribes E, Carriere D, Goubet C, Galiegue S, Casellas P, Simony-Lafontaine J. Immunohistochemical assessment of the peripheral benzodiazepine receptor in human tissues. J Histochem Cytochem 2004;52:19–28.
[8] Brody AL, Hubert R, Enoki R, Garcia LY, Mamoun MS, Okita K, London ED, Nurmi EL, Seaman LC, Mandelkern MA. Effect of cigarette smoking on a marker for neuroinflammation: a [11C]DAA1106 positron emission tomography study. Neuropsychopharmacology 2017;42:1630–9.
[9] Cipriano P, Yoon D, Gandhi H, Holley D, Thakur D, Ith M, Hargreaves B, Kennedy D, Smuck M, Cheng I, Biswal S. (18)F-FDG PET/MRI in chronic sciatica: early results revealing spinal and non-spinal abnormalities. J Nucl Med 2017. doi: 10.2967/jnumed.117.198259. [Epub ahead of print].
[10] Clark AK, Gentry C, Bradbury EJ, McMahon SB, Malcangio M. Role of spinal microglia in rat models of peripheral nerve injury and inflammation. Eur J Pain 2007;11:223–30.
[11] Cohen SP, Bicket MC, Jamison D, Wilkinson I, Rathmell JP. Epidural steroids: a comprehensive, evidence-based review. Reg Anesth Pain Med 2013;38:175–200.
[12] Costa B, Pini S, Gabelloni P, Da Pozzo E, Abelli M, Lari L, Preve M, Lucacchini A, Cassano GB, Martini C. The spontaneous Ala147Thr amino acid substitution within the translocator protein influences pregnenolone production in lymphomonocytes of healthy individuals. Endocrinology 2009;150:5438–45.
[13] De Leener B, Levy S, Dupont SM, Fonov VS, Stikov N, Louis Collins D, Callot V, Cohen-Adad J. SCT: Spinal Cord Toolbox, an open-source software for processing spinal cord MRI data. Neuroimage 2017;145(pt A):24–43.
[14] Guo W, Wang H, Watanabe M, Shimizu K, Zou S, LaGraize SC, Wei F, Dubner R, Ren K. Glial-cytokine-neuronal interactions underlying the mechanisms of persistent pain. J Neurosci 2007;27:6006–18.
[15] Hains BC, Waxman SG. Activated microglia contribute to the maintenance of chronic pain after spinal cord injury. J Neurosci 2006; 26:4308–17.
[16] Herranz E, Gianni C, Louapre C, Treaba CA, Govindarajan ST, Ouellette R, Loggia ML, Sloane JA, Madigan N, Izquierdo-Garcia D, Ward N, Mangeat G, Granberg T, Klawiter EC, Catana C, Hooker JM, Taylor N, Ionete C, Kinkel RP, Mainero C. Neuroinflammatory component of gray matter pathology in multiple sclerosis. Ann Neurol 2016;80:776–90.
[17] Hirvonen J, Kreisl WC, Fujita M, Dustin I, Khan O, Appel S, Zhang Y, Morse C, Pike VW, Innis RB, Theodore WH. Increased in vivo expression of an inflammatory marker in temporal lobe epilepsy. J Nucl Med 2012;53: 234–40.
[18] Imaizumi M, Briard E, Zoghbi SS, Gourley JP, Hong J, Fujimura Y, Pike VW, Innis RB, Fujita M. Brain and whole-body imaging in nonhuman primates of [11C]PBR28, a promising PET radioligand for peripheral benzodiazepine receptors. Neuroimage 2008;39:1289–98.
[19] Ji RR, Berta T, Nedergaard M. Glia and pain: is chronic pain a gliopathy? PAIN 2013;154(suppl 1):S10–28.
[20] Kosek E, Martinsen S, Gerdle B, Mannerkorpi K, Lofgren M, Bileviciute-Ljungar I, Fransson P, Schalling M, Ingvar M, Ernberg M, Jensen KB. The translocator protein gene is associated with symptom severity and cerebral pain processing in fibromyalgia. Brain Behav Immun 2016;58: 218–27.
[21] Kreisl WC, Jenko KJ, Hines CS, Lyoo CH, Corona W, Morse CL, Zoghbi SS, Hyde T, Kleinman JE, Pike VW, McMahon FJ, Innis RB; Biomarkers Consortium PETRPT. A genetic polymorphism for translocator protein 18 kDa affects both in vitro and in vivo radioligand binding in human brain to this putative biomarker of neuroinflammation. J Cereb Blood Flow Metab 2013;33:53–8.
[22] Lacor P, Benavides J, Ferzaz B. Enhanced expression of the peripheral benzodiazepine receptor (PBR) and its endogenous ligand octadecaneuropeptide (ODN) in the regenerating adult rat sciatic nerve. Neurosci Lett 1996;220:61–5.
[23] Latremoliere A, Latini A, Andrews N, Cronin SJ, Fujita M, Gorska K, Hovius R, Romero C, Chuaiphichai S, Painter M, Miracca G, Babaniyi O, Remor AP, Duong K, Riva P, Barrett LB, Ferreiros N, Naylor A, Penninger JM, Tegeder I, Zhong J, Blagg J, Channon KM, Johnsson K, Costigan M, Woolf CJ. Reduction of neuropathic and inflammatory pain through inhibition of the tetrahydrobiopterin pathway. Neuron 2015;86: 1393–406.
[24] LeBlanc BW, Zerah ML, Kadasi LM, Chai N, Saab CY. Minocycline injection in the ventral posterolateral thalamus reverses microglial reactivity and thermal hyperalgesia secondary to sciatic neuropathy. Neurosci Lett 2011;498:138–42.
[25] Liu X, Li W, Dai L, Zhang T, Xia W, Liu H, Ma K, Xu J, Jin Y. Early repeated administration of progesterone improves the recovery of neuropathic pain and modulates spinal 18kDa-translocator protein (TSPO) expression. J Steroid Biochem Mol Biol 2014;143:130–40.
[26] Liu X, Liu H, Xu S, Tang Z, Xia W, Cheng Z, Li W, Jin Y. Spinal translocator protein alleviates chronic neuropathic pain behavior and modulates spinal astrocyte-neuronal function in rats with L5 spinal nerve ligation model. PAIN 2016;157:103–16.
[27] Loggia ML, Chonde DB, Akeju O, Arabasz G, Catana C, Edwards RR, Hill E, Hsu S, Izquierdo-Garcia D, Ji RR, Riley M, Wasan AD, Zurcher NR, Albrecht DS, Vangel MG, Rosen BR, Napadow V, Hooker JM. Evidence for brain glial activation in chronic pain patients. Brain 2015;138:604–15.
[28] Lyoo CH, Ikawa M, Liow JS, Zoghbi SS, Morse CL, Pike VW, Fujita M, Innis RB, Kreisl WC. Cerebellum can serve as a pseudo-reference region in alzheimer disease to detect neuroinflammation measured with PET radioligand binding to translocator protein. J Nucl Med 2015;56:701–6.
[29] McMahon SB, La Russa F, Bennett DL. Crosstalk between the nociceptive and immune systems in host defence and disease. Nat Rev Neurosci 2015;16:389–402.
[30] Meller ST, Dykstra C, Grzybycki D, Murphy S, Gebhart GF. The possible role of glia in nociceptive processing and hyperalgesia in the spinal cord of the rat. Neuropharmacology 1994;33:1471–8.

[31] Mika J. Modulation of microglia can attenuate neuropathic pain symptoms and enhance morphine effectiveness. Pharmacol Rep 2008; 60:297–307.
[32] Nahin RL. Estimates of pain prevalence and severity in adults: United States, 2012. J Pain 2015;16:769–80.
[33] Nair A, Veronese M, Xu X, Curtis C, Turkheimer F, Howard R, Reeves S. Test-retest analysis of a non-invasive method of quantifying [(11)C]-PBR28 binding in Alzheimer's disease. EJNMMI Res 2016;6:72.
[34] Okada-Ogawa A, Suzuki I, Sessle BJ, Chiang CY, Salter MW, Dostrovsky JO, Tsuboi Y, Kondo M, Kitagawa J, Kobayashi A, Noma N, Imamura Y, Iwata K. Astroglia in medullary dorsal horn (trigeminal spinal subnucleus caudalis) are involved in trigeminal neuropathic pain mechanisms. J Neurosci 2009;29:11161–71.
[35] Owen DR, Yeo AJ, Gunn RN, Song K, Wadsworth G, Lewis A, Rhodes C, Pulford DJ, Bennacef I, Parker CA, StJean PL, Cardon LR, Mooser VE, Matthews PM, Rabiner EA, Rubio JP. An 18-kDa translocator protein (TSPO) polymorphism explains differences in binding affinity of the PET radioligand PBR28. J Cereb Blood Flow Metab 2012;32:1–5.
[36] Paganoni S, Alshikho MJ, Zurcher NR, Cernasov P, Babu S, Loggia ML, Chan J, Chonde DB, Garcia DI, Catana C, Mainero C, Rosen BR, Cudkowicz ME, Hooker JM, Atassi N. Imaging of glia activation in people with primary lateral sclerosis. NeuroImage Clin 2018;17:347–53.
[37] Raghavendra V, Rutkowski MD, DeLeo JA. The role of spinal neuroimmune activation in morphine tolerance/hyperalgesia in neuropathic and sham-operated rats. J Neurosci 2002;22:9980–9.
[38] Raghavendra V, Tanga F, DeLeo JA. Inhibition of microglial activation attenuates the development but not existing hypersensitivity in a rat model of neuropathy. J Pharmacol Exp Ther 2003;306:624–30.
[39] Saal JS, Franson RC, Dobrow R, Saal JA, White AH, Goldthwaite N. High levels of inflammatory phospholipase A2 activity in lumbar disc herniations. Spine (Phila Pa 1976) 1990;15:674–8.
[40] Sayenko DG, Atkinson DA, Dy CJ, Gurley KM, Smith VL, Angeli C, Harkema SJ, Edgerton VR, Gerasimenko YP. Spinal segment-specific transcutaneous stimulation differentially shapes activation pattern among motor pools in humans. J Appl Physiol (1985) 2015;118:1364–74.
[41] Simon LS. Relieving pain in America: a blueprint for transforming prevention, care, education, and research. J Pain Palliat Care Pharmacother 2012;26:197–8.
[42] Taylor AM, Mehrabani S, Liu S, Taylor AJ, Cahill CM. Topography of microglial activation in sensory- and affect-related brain regions in chronic pain. J Neurosci Res 2017;95:1330–5.
[43] Tsuda M, Shigemoto-Mogami Y, Koizumi S, Mizokoshi A, Kohsaka S, Salter MW, Inoue K. P2X4 receptors induced in spinal microglia gate tactile allodynia after nerve injury. Nature 2003;424:778–83.
[44] Turkheimer FE, Rizzo G, Bloomfield PS, Howes O, Zanotti-Fregonara P, Bertoldo A, Veronese M. The methodology of TSPO imaging with positron emission tomography. Biochem Soc Trans 2015;43: 586–92.
[45] Vanelderen P, Rouwette T, Kozicz T, Heylen R, Van Zundert J, Roubos EW, Vissers K. Effects of chronic administration of amitriptyline, gabapentin and minocycline on spinal brain-derived neurotrophic factor expression and neuropathic pain behavior in a rat chronic constriction injury model. Reg Anesth Pain Med 2013;38:124–30.
[46] Vanelderen P, Van Zundert J, Kozicz T, Puylaert M, De Vooght P, Mestrum R, Heylen R, Roubos E, Vissers K. Effect of minocycline on lumbar radicular neuropathic pain: a randomized, placebo-controlled, double-blind clinical trial with amitriptyline as a comparator. Anesthesiology 2015;122:399–406.
[47] Watkins LR, Martin D, Ulrich P, Tracey KJ, Maier SF. Evidence for the involvement of spinal cord glia in subcutaneous formalin induced hyperalgesia in the rat. PAIN 1997;71:225–35.
[48] Wei XH, Wei X, Chen FY, Zang Y, Xin WJ, Pang RP, Chen Y, Wang J, Li YY, Shen KF, Zhou LJ, Liu XG. The upregulation of translocator protein (18 kDa) promotes recovery from neuropathic pain in rats. J Neurosci 2013;33:1540–51.
[49] Wuertz K, Haglund L. Inflammatory mediators in intervertebral disk degeneration and discogenic pain. Glob Spine J 2013;3:175–84.
[50] Zhou X, Cipriano P, Kim B, Dhatt H, Rosenberg J, Mittra E, Do B, Graves E, Biswal S. Detection of nociceptive-related metabolic activity in the spinal cord of low back pain patients using (18)F-FDG PET/CT. Scand J Pain 2017;15:53–7.
[51] Zurcher NR, Loggia ML, Lawson R, Chonde DB, Izquierdo-Garcia D, Yasek JE, Akeju O, Catana C, Rosen BR, Cudkowicz ME, Hooker JM, Atassi N. Increased in vivo glial activation in patients with amyotrophic lateral sclerosis: assessed with [(11)C]-PBR28. Neuroimage Clin 2015;7: 409–14.